VIA MEDICA

ORIGINAL ARTICLE

Acta Angiol
Vol. 30, No. 4, pp. 131–145
DOI: 10.5603/aa.99725

ISSN 1234–950X
e-ISSN 1644–3276

Consequences of the presence of atherosclerotic lesions within the thoracic aorta during a car crash — a finite element method study

Oliwia Kolaszynska[1], Lukasz Lacny[2], Jacek Lorkowski[3, 4]

[1]I Department of Internal Medicine, Asklepios Klinikum Uckermark, Am Klinikum 1, Germany

[2]Cracow University of Technology, Krakow, Poland

[3]University of Surrey, Surrey Institute for People-Centred AI (PAI), Giuldford, Surrey GU2 7XH, UK

[4]Central Clinical Hospital of the Ministry of Interior, Warsaw, Poland

Abstract

Atherosclerosis has been shown to alter vascular properties and predispose to injury. Blunt aortic trauma (BAT) is responsible for 20% of vehicle-related deaths. This work aims to demonstrate and better understand the biomechanics of the aorta with and without atherosclerotic changes during a frontal car crash using a finite element method (FEM). Secondarily, the influence of blood pressure was evaluated. A FEM model was created with an ANSYS system based on computed tomography images of 44 patients. The distribution of stress and deformation varies according to the stage of atherosclerotic disease. Finally, at a speed of 30 km/h, an aortic rupture occurs. The presence of a calcified atherosclerotic plaque in the thoracic aorta at an advanced and calcified stage increases its susceptibility to rupture during a car crash. No effect of blood pressure on aortic biomechanics was observed.

Keywords: atherosclerosis, aorta, biomechanics, car crash

Acta Angiol 2024; 30, 4: 131–145

Introduction

Blunt aortic trauma (BAT) is responsible for approx. 20% of vehicle-related deaths and is associated with a high mortality rate due to blunt traumatic aortic rupture (BTAR) or blunt traumatic aortic injury (BTAI) [1, 2]. The aortic isthmus is the site of most BTAR/BTAI. This part of the aorta, as a "transition zone" between a secured descending aorta and an unsecured ascending aorta, appears to be most exposed to trauma due to the forces of bending, torsion, and tension [1]. The nature of the trauma is important, as is the structure of the aorta itself. Atherosclerotic lesions occur in arteries with low wall shear stress and high oscillatory stress values [3]. In a healthy state, the inner layer of the aorta consists of endothelial cells. The biomechanics change with the accumulation of other cells such as smooth muscle cells, collagen and elastin fibers, adipocytes, foam cells, and finally calcifications or blood cells. The vascular smooth muscle cells and their differentiation within the aorta are unique. Proteomic studies have described 232 proteins present in the aorta that are specific to the aorta [4]. These phenotypic changes may predispose to atherosclerotic lesions. Atherosclerosis itself has been shown to increase arterial stiffness and predispose to intimal rupture and injury [5–7].

Address for correspondence: Oliwia Kolaszynska MD, I Department of Internal Medicine, Asklepios Klinikum Uckermark, Am Klinikum 1, 16303 Schwedt (Oder), Germany, e-mail: oliwia.kolaszynska@gmail.com

Recieved: 10.03.2024; Accepted: 13.11.2024; Early publication date: 6.12.2024

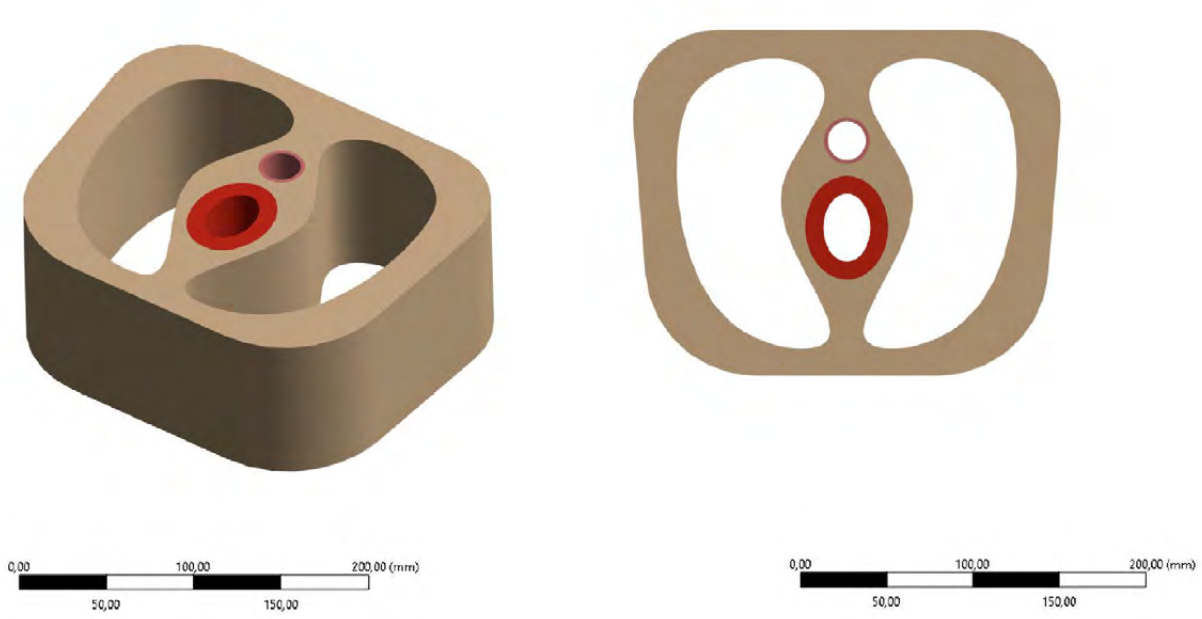

Figure 1. The initial model of a thorax cavity

This paper aims to present a finite element model of polytrauma and its influence on human vascular tissue, represented by the thoracic aorta, in a healthy and atherosclerotic state. The second aspect was to analyze the influence of systolic blood pressure on the biomechanics of the aorta during a car crash. This work should provide a future solution for further biomechanical analysis of human vascular tissue.

Material and methods

The study protocol conforms to the ethical guidelines of the 1975 Declaration of Helsinki. Approval of the institutional ethics commission has been obtained for this study (Decision number 33/2019 of 13.02.2019).

Exclusion criteria. According to the 2014 ESC guidelines of aortic diseases [8], patients are eligible for surgical treatment of aortic aneurysms with an aortic diameter of 55 mm, and in some justified cases (e.g., bicuspid aortic valve, Marfan syndrome, growth > 2 mm/year) with an aortic diameter of 50 mm. Only patients with an aortic diameter ≤ 50 mm were included in further analyses. Also, patients with a known neoplastic process within the thorax cavity, suspicious thoracic lesions, after cardiothoracic surgery, with coarctation of the aorta or other specific anomalies, or with a history of a connective tissue disease have been excluded from further analyses.

In silico analyses have been performed with ANSYS and have been based on computed tomography (CT) images of 44 patients treated in the Independent Public Regional Hospital in Szczecin, Poland in years 12.2015–12.2022.

Due to the complexity of a thorax and the high computing power required to create an FE- model, the authors have created an initial model of a thorax. A simplified scheme is shown in Figure 1. Based on this model, the biomechanical properties of bones and internal organs were used to create a gel into which an aorta was placed.

The thorax has been modeled with material properties given in Table 1. It was assumed that the pressure within the thoracic aorta is 100, 115, and 125 mmHg. Due to data discrepancies, the pressure in the thoracic cavity was modeled as 1 atmosphere.

Atherosclerotic plaques have been modeled at different stages of atherosclerotic disease. The thickening of the vessel wall due to plaque progression was also considered and divided into stages. Assuming that the intima occupies approximately 3% of the aortic wall thickness in healthy conditions, stages 1, 2, 3, and 4 result in intima growth to 5%, 20%, 50%, and 80% of the arterial wall thickness, respectively. For simplicity, the atherosclerotic plaque model has been restricted to the intima.

Stage 1 represents a lipid tissue covering 25% of the aortic wall with 5% intimal growth in cross-section. Stage 2 was modeled as lipid tissue covering 50% of the aortic wall with 5% (covering 25% of the aortic wall) and 20% (covering 25% of the aortic wall) intimal

Table 1. Material properties of the structures of a thoracic cavity

Tissue	Young modulus	Poisson's ratio
Ribs [9, 10]	10–17 GPa	0.3
Sternum [9, 10]	10–17 GPa	0.3
Thoracic spine [11]	19.7 GPa	0.3
Aorta [12]	7.5 MPa	0.45
Heart wall [13, 14]	480 MPa	0.4
Red blood cells [15, 16]	26 kPa	0.49
White blood cells [17]	16 MPa	0.49
Platelets [17]	1–15 kPa	0.49
Lungs [18–20]	3.55 kPa	0.4
Oesophagus [21]	480 MPa	0.5
Adipose tissue [22]	1.3 MPa	0.49
Gel	120 MPa	0.35

growth in cross-section. Stage 3 covers 75% of the aortic wall in cross-section and contains lipid (25% with 5% and 20% intimal growth) and fibrotic (25%) tissue. Stage 4 covers 100% of the aortic wall in cross-section and consists of: the lipid tissue (25% with 5% and 20% intimal growth), fibrotic tissue (25%), and calcified tissue (25%). The simplified scheme is shown in Figure 2. Material properties have been based on the work of Carrera et al. [23] and are presented in Table 2.

The next step was to simulate a frontal car crash at the following speeds: 15 km/h, 20 km/h, 25 km/h, and 30 km/h for each stage. In addition, three models have been created for the 15 km/h speed (at each level) with increasing systolic blood pressure of 115 mmHg and 125 mmHg.

Results

The general scheme common to all configurations results in the aorta bending from anterior to posterior (due to the force applied anteriorly). In all cases, there is a deformation of the thoracic cavity which increases with time. The elastic strain reaches its maximum within the first few seconds and then decreases. The model for healthy conditions at a speed of 15 km/h is shown in Figures 3 and 4.

Healthy conditions. Initial localization of maximum stress and deformation can be observed on the distal end of the vessel at a speed of 15 km/h. This pattern changes and results in centrally located highest stresses and deformation at a speed of 30 km/h. Deformation increases and the highest stress values are observed at a speed of 20 km/h. Changes are presented in Figures 5, 6, 11, and 12.

Stage 1. Deformations and stresses increase without time displacement. At the speed of 15 km/h, the highest stresses and deformation occur within the left and posterior aortic walls. At the speed of 30 km/h forces acting on the right aortic wall increase. Forces acting on the posterior and both lateral walls increase. The lowest values can be observed on the front aortic wall. Changes are presented in Figures 7, 8, 13 and 14.

Stage 2. Deformations and stresses increase with a small-time shift.

Stage 3. Deformation reaches lower initial values with increasing tendency. Stresses become higher.

Stage 4. Initially "spilled" maximum stress and deformation at the posterior and lateral wall is localized on the anterior aortic wall. Stresses and deformations increase and finally reach their highest values at the end of a simulation leading to aortic rupture on the anterior aortic wall. Changes are presented in Figures 9, 10, 15 and 16.

A comparison of the differences in deformation and stress between healthy aorta and stage 4 is shown in Figure 17. Aortic rupture is shown in Figure 18.

Discussion

The human thorax is a structure complicated to model. Wang was the first to present a finite element model of a human thorax presenting not only bone tissue but also organs and vasculature [24, 25]. Shah et al. were the first to create a FEM model of an aorta and its rupture during a chest impact [26]. Followed by other authors, the first models have been proposed to model biomechanical factors of aortic tissue [26, 27]. Firstly, it should be explained that deformation (caused by a given force acting on a body) is expressed as strain. The strain is useful in determining the exact elongation or tension a structure may experience under certain loading conditions. Stress, on the other hand, determi-

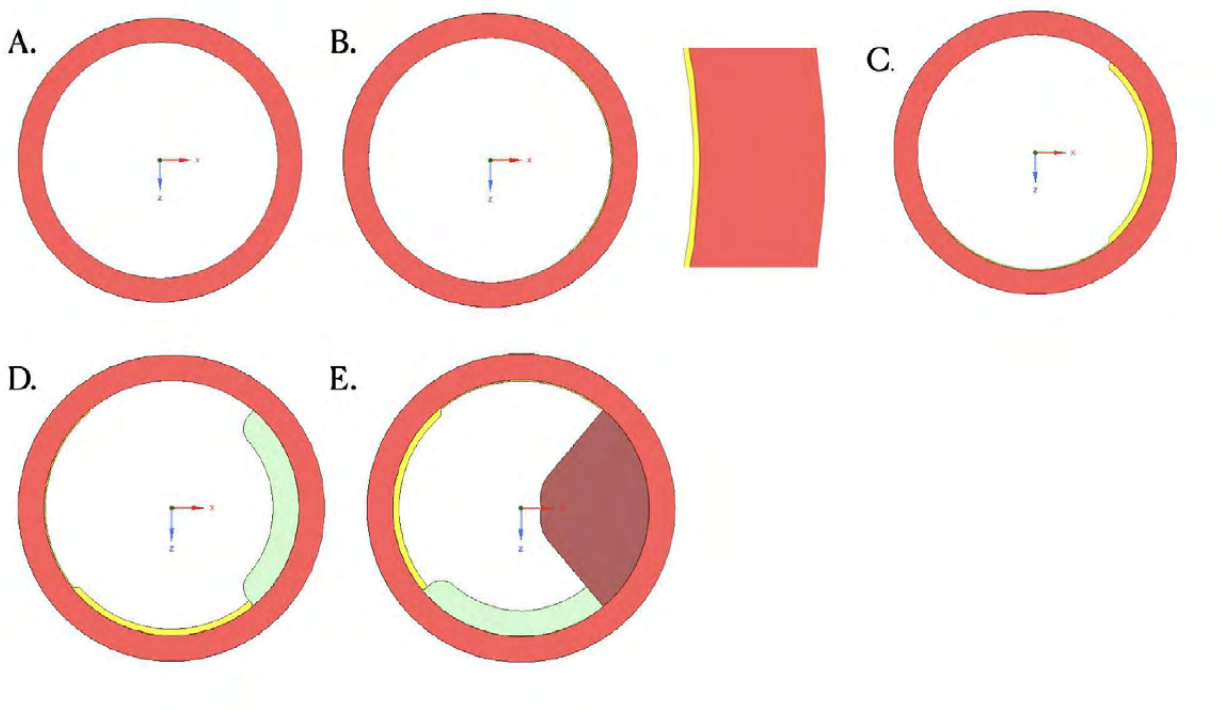

Figure 2. Stages of an atherosclerotic Plaque. **A.** Healthy aorta; **B.** Stage I with cross-section; **C.** Stage 2; **D.** Stage 3; **E.** Stage 4. Colours represent particular tissues. Yellow-lipid tissue. Green-fibrotic tissue. Brown-calcified tissue

Table 2. The biomechanical properties of modeled materials

Tissue	Young's modulus [MPa]	Poisson's ratio
Lipid	0.10	0.33
Fibrous	2.40	0.33
Calcified	12.00	0.33
Tunica media	1.00	0.33

nes the state of a structure under external loads. The von Mises stress is introduced in this paper. In this case, it is used to describe the yielding of the aorta under loading conditions at the point of maximum principal strain and is considered to represent a potential failure of aortic integrity.

Interestingly, the aorta has been considered as a "deformable elastic structure with stresses dependent on transmural pressure" [28]. It has been shown that the diameter of the aorta changes with the systolic blood pressure [29, 30]. Vasava et. al have presented a finite element method study for hyper- and hypotension [31]. However, the study was designed to describe a blood flow pattern and stresses within the thoracic aorta and its main branches. In this study, it was shown that an increase of blood pressure up to 145 mmHg within the thoracic aorta has no relevant impact on the biomechanics of the thoracic aorta at a speed of 15 km/h. The influence of pressure should be further evaluated in the future for higher speed values.

Little data is describing a BAT within the thoracic aorta and the mechanism of BAT remains unclear [32–34]. Proposed explanations include disruption of the aorta from within by hypertension, sudden stretching of an arterial wall with subsequent rupture at the site of presumed weakness (isthmus), diaphragmatic aortic occlusion, a sudden increase in intrathoracic pressure acting on the heart and great vessels through the bony structures of the thoracic cavity, upward displacement of the heart, and a combination of the above mechanisms [32, 33, 35–37]. Some authors claim that trauma places the aorta in a highly vulnerable state and that the deformation of a vessel is the direct initiator of injury [1]. Constantly changing conditions, dynamics, and many computations suggest that *in silico* modeling is an appropriate direction to study BAT. To fully understand BAT, the mechanics of the aortic wall should be studied in detail. To the best of our knowledge, this is the first paper to describe the forces acting within the thoracic aorta with and without atherosclerotic lesions during trauma.

There are 6 basic types of atherosclerotic lesions: type I — initial plaque, type II — fatty streak, type

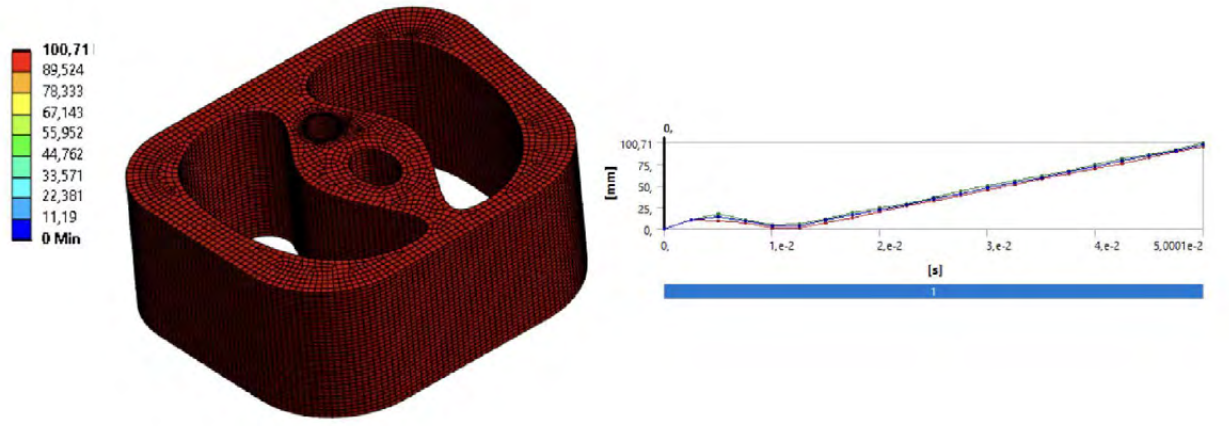

Figure 3. Deformation under healthy conditions at a speed of 15 km/h

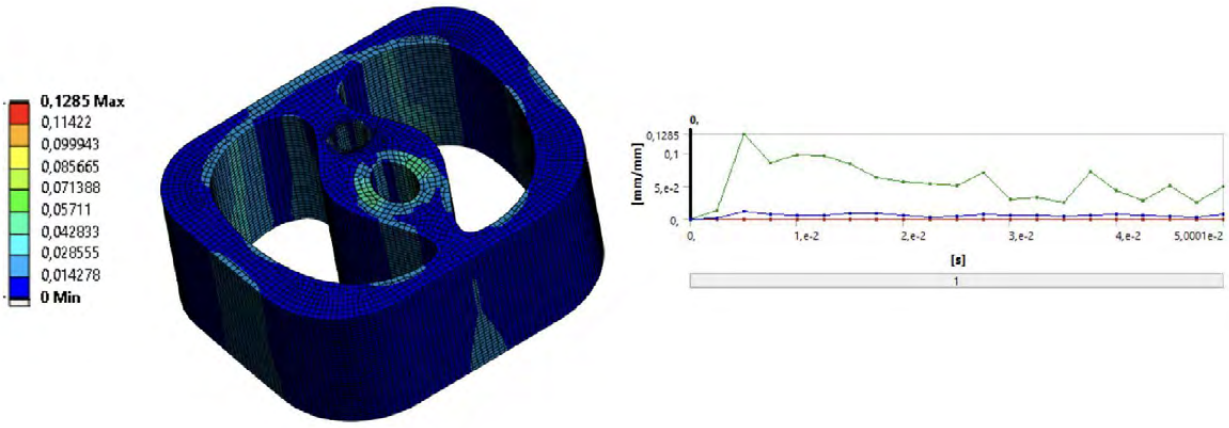

Figure 4. Elastic strain under healthy conditions at a speed of 15 km/h

III — intermediate lesion or pre-atheroma, type IV — atheroma, type V — fibro-atheroma, and type VI — a ruptured lesion that can transform into type VII — calcified lesion or type VIII — fibrotic lesion [38, 39]. Along with the accumulation of other cells with different biomechanical properties, the biomechanics of the aortic wall alters. Kozun et al. [5] point out that Young's modulus of a single collagen fiber is higher compared to fibrosis within an atherosclerotic lesion. The authors have studied the influence of atherosclerosis in its different stages on aortic dissection. They have shown that the lowest values occur within stage IV lesions, which may make the aorta most susceptible to dissection. In our study, lesions with a calcified plaque component led to aortic rupture. Another pathological study of 8 cadavers with traumatic aortic rupture showed that longitudinal stretching of the aorta was the main cause of injury. Atherosclerotic changes within the aorta have also been shown to promote injury [40]. Increasing age is one of the risk factors for BAT [37]. Current trends and constantly growing amounts of data require special solutions and the application of artificial intelligence in their processing [41]. Recently, attempts have been made to combine a FE- method with artificial intelligence (deep neural networks) [42].

There are two methods of stress application — indentation and tensile. Indentation has also been shown to give lower values of Young's modulus in soft tissues [43]. Unfortunately, unified material properties of tissues, including those within a thoracic cavity, are not available. In addition, material properties vary between different items depending on the test conditions, and the age or sex of the specimen [24]. In conclusion, test conditions should be standardized and more rigorous.

Most chest injuries with fatal aortic rupture occur at speeds greater than 33 km/h [44, 45]. This finding

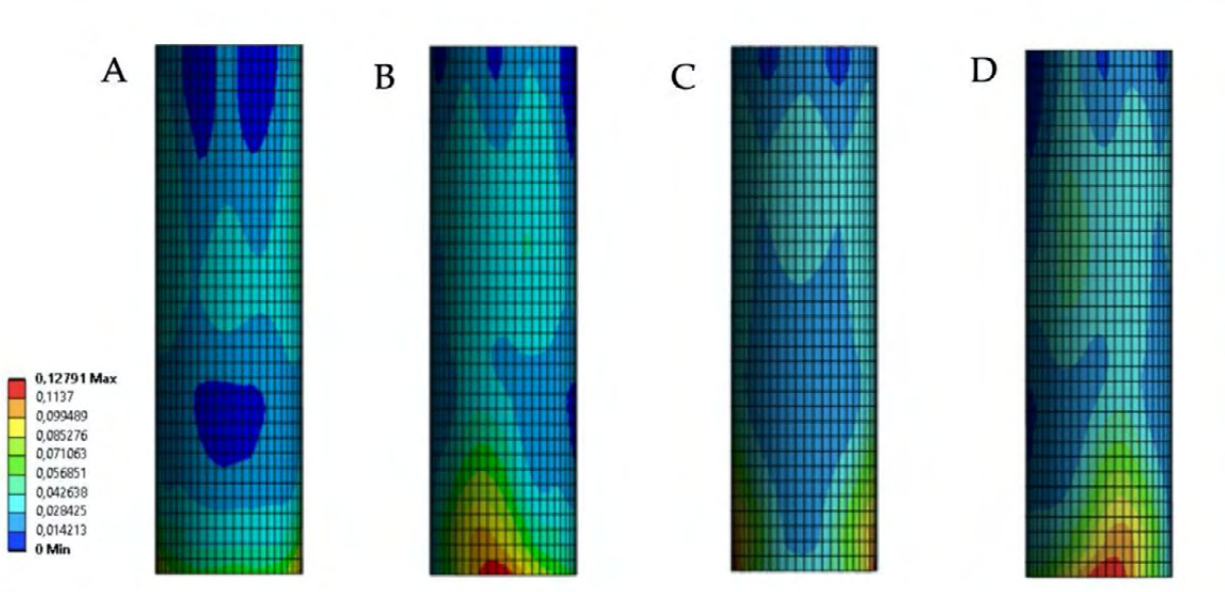

Figure 5. Maximum stresses in an aortic wall in healthy conditions at the speed of 15 km/h. A — aortic front wall; B — left wall; C — posterior wall; D — right wall

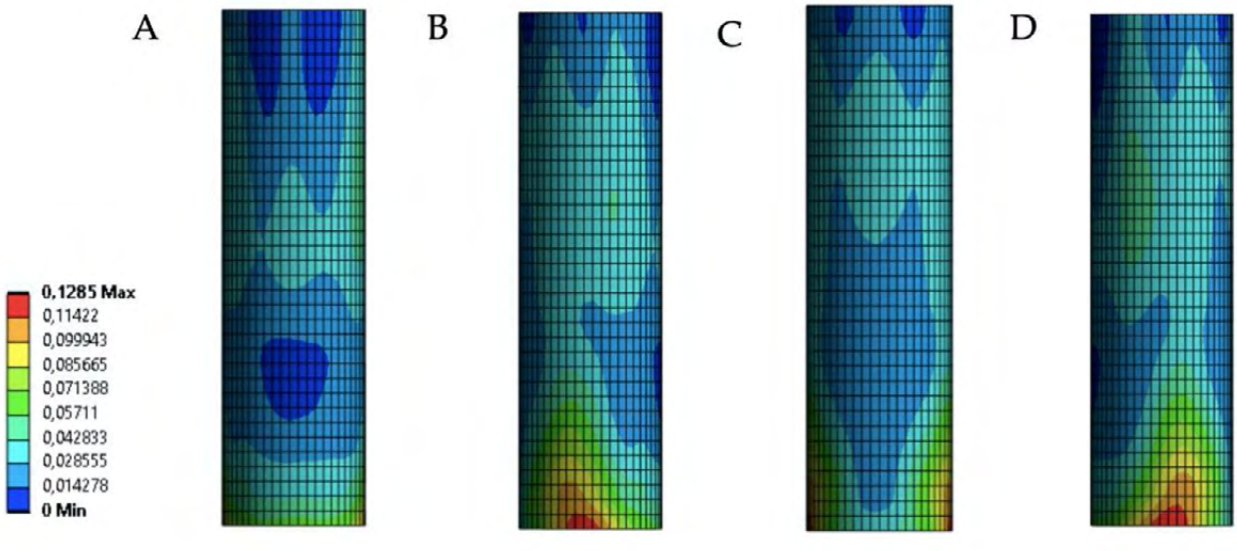

Figure 6. Maximum deformation of an aortic wall in healthy conditions at the speed of 15 km/h. A — aortic front wall; B — left wall; C — posterior wall; D — right wall

has been confirmed in our study. Some authors have presented an FE model of the aorta during a frontal impact [25], but none of these articles analyzed the presence of atherosclerotic tissue. In this study, the authors present an *in silico* model of aortic rupture during a car crash.

Limitations. Our paper presents an *in silico* model of the aorta in a simplified form of a straightened pipe, preserving all the biomechanical properties of aortic tissue. The main objective of this study, as a first step in the biomechanical analysis of the aorta, was to determine the influence of the presence of an atherosclerotic plaque itself on the behavior of the vascular tissue in polytrauma. According to the authors, it is necessary to first consider the isolated factor of atherosclerosis and its effect on the biomechanics of the vessel, and only

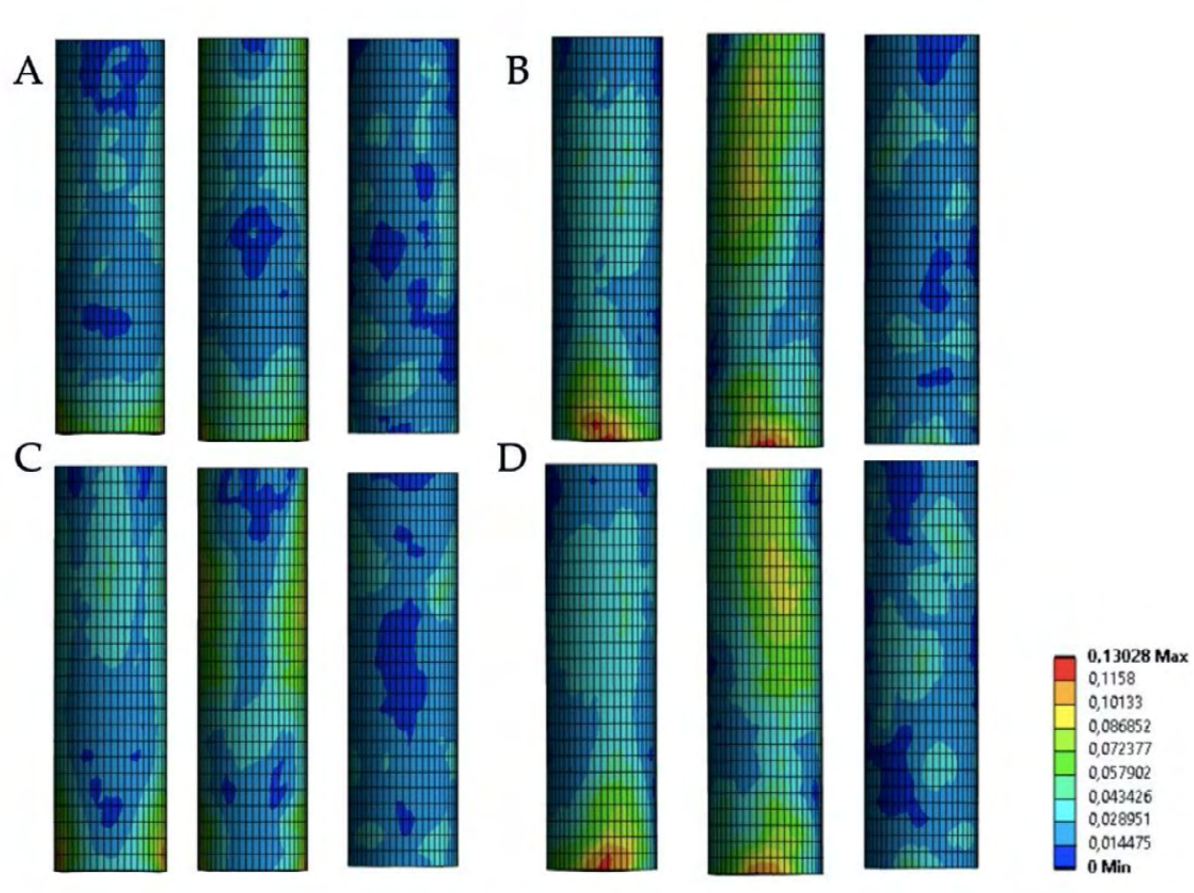

Figure 7. Maximum stresses in an aortic wall in stage 1 within the first second after impact at 15 km/h. A — aortic front wall; B — left wall; C — posterior wall; D — right wall

then to assess the shape of the aorta. Skipping one of the steps in this analysis could lead to erroneous conclusions. Therefore, this article only considers the model of atherosclerosis at different stages of progression within the vessel wall. Similar models with anatomical curvatures and aortic branches as well as longitudinal forces should be the next direction to assess the influence of polytrauma on the human atherosclerotic aorta.

The presence of a safety belt was not evaluated in this study.

In addition, the aortic wall is described as inhomogeneous with non-linear anisotropic mechanical properties. As mentioned above, no study has evaluated the biomechanical properties of the aorta in vivo. Therefore, a simplified model of the aortic wall has been presented.

This study presents a theoretical model of the behavior of aortic tissue with and without atherosclerosis and should be further developed in the future to provide new solutions for the treatment and monitoring of patients with blunt aortic trauma.

Conclusions

The presence of a calcified atherosclerotic plaque within the thoracic aorta increases its vulnerability to rupture during a car crash. The change in biomechanics found in the finite element method analysis is more intensified not with low-grade atherosclerotic lesions but in advanced atherosclerosis with calcified atherosclerotic foci occurring within it. In addition, the authors found no relevant correlation between an increase in systolic blood pressure (even within the normal range) and altered stress patterns within the thoracic aorta. This description may contribute to a better understanding and visualization of complicated aortic trauma.

Secondly, these models can be used in planning medical treatment or improving already existing guidelines for polytrauma involving the aorta. The thoracic aorta is a specific structure requiring a strong computational power. The authors forecast that this paper will contribute to providing future solutions and the development of complicated *in-silico* simulations.

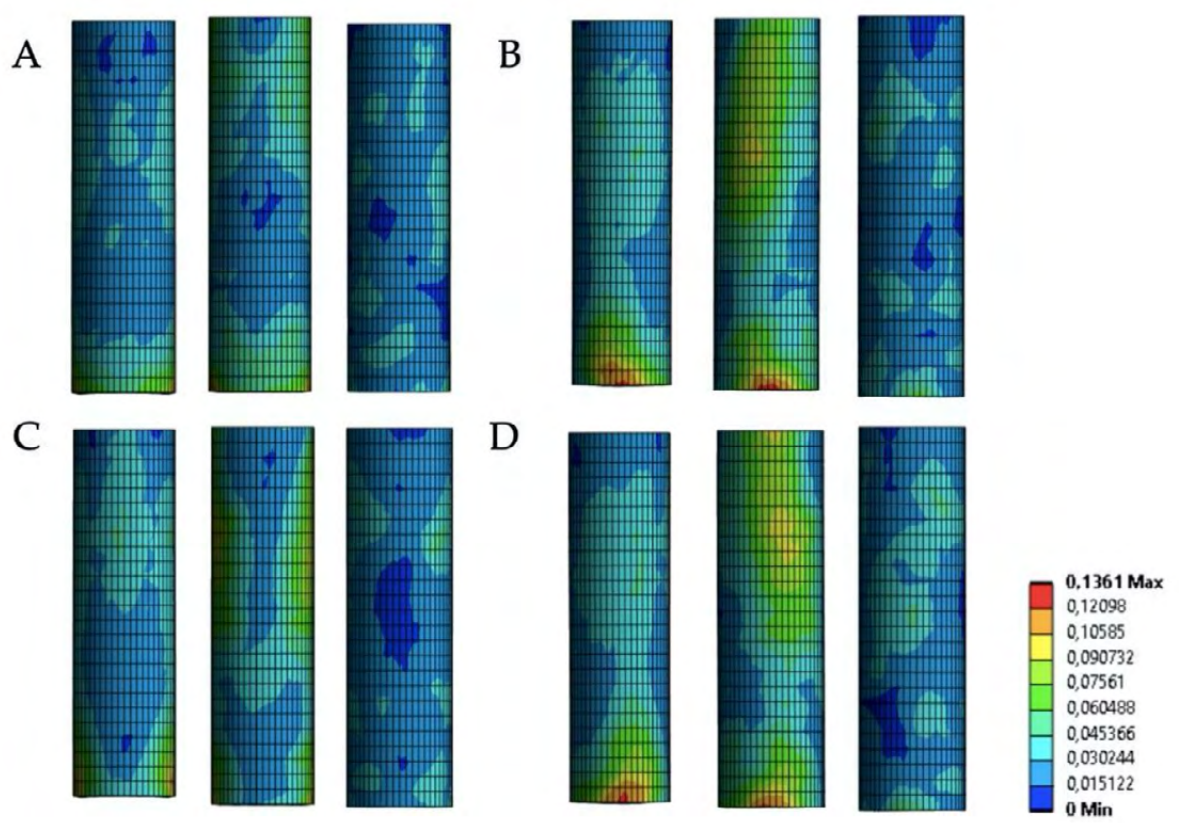

Figure 8. Maximum deformation of an aortic wall in stage 1 within the first second after impact at 15 km/h. A — aortic front wall; B — left wall; C — posterior wall; D — right wall

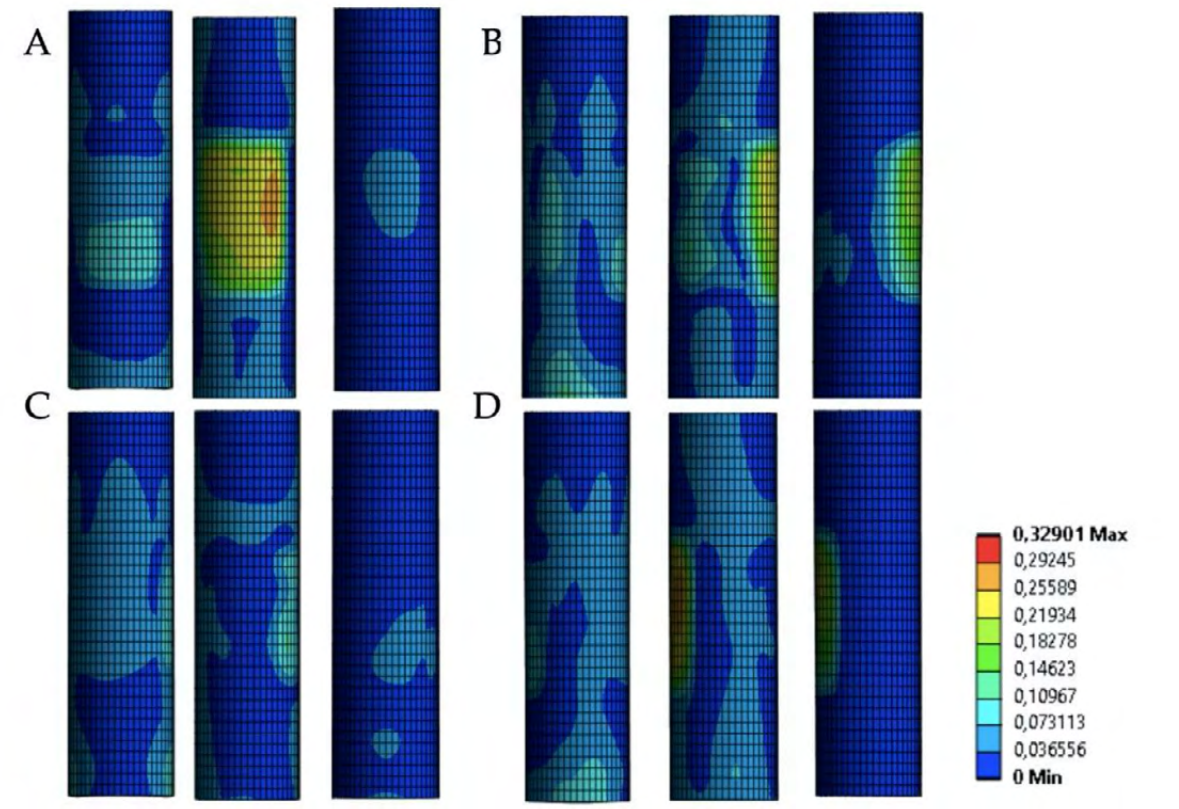

Figure 9. Maximum stresses in an aortic wall in stage 4 within the first second after impact at 15 km/h. A — aortic front wall; B — left wall; C — posterior wall; D — right wall

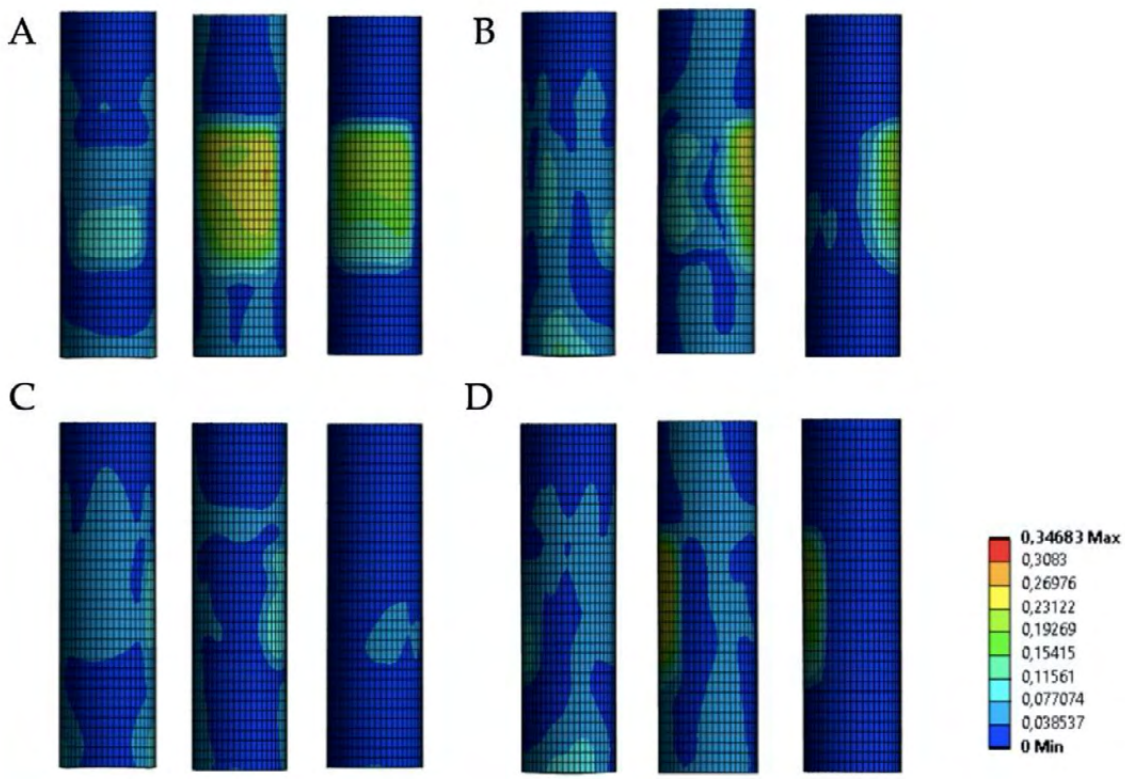

Figure 10. Maximum deformation of an aortic wall in stage 4 within the first second after impact at 15 km/h. A — aortic front wall; B — left wall; C — posterior wall; D — right wall

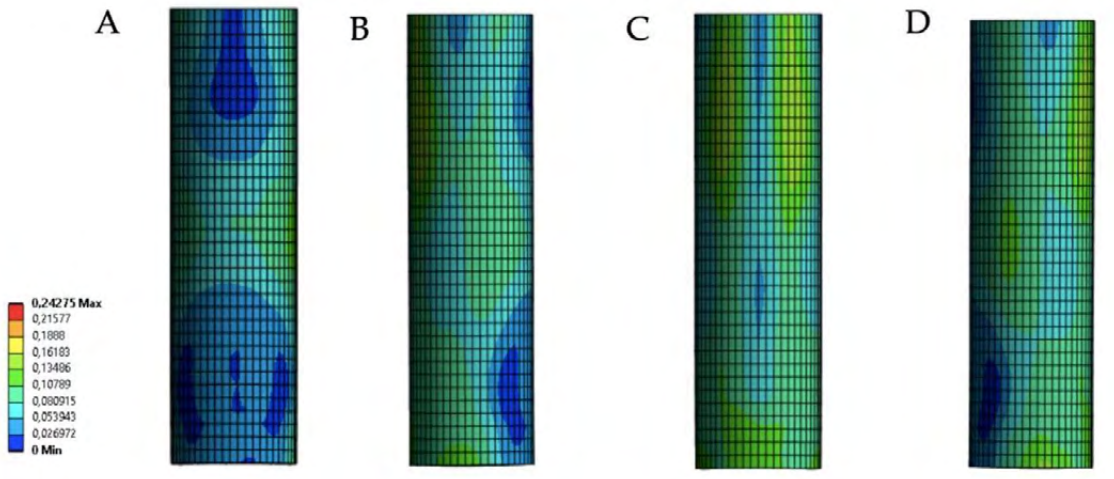

Figure 11. Maximum stresses in an aortic wall in healthy conditions at the speed of 30 km/h. A — aortic front wall; B — left wall; C — posterior wall; D — right wall

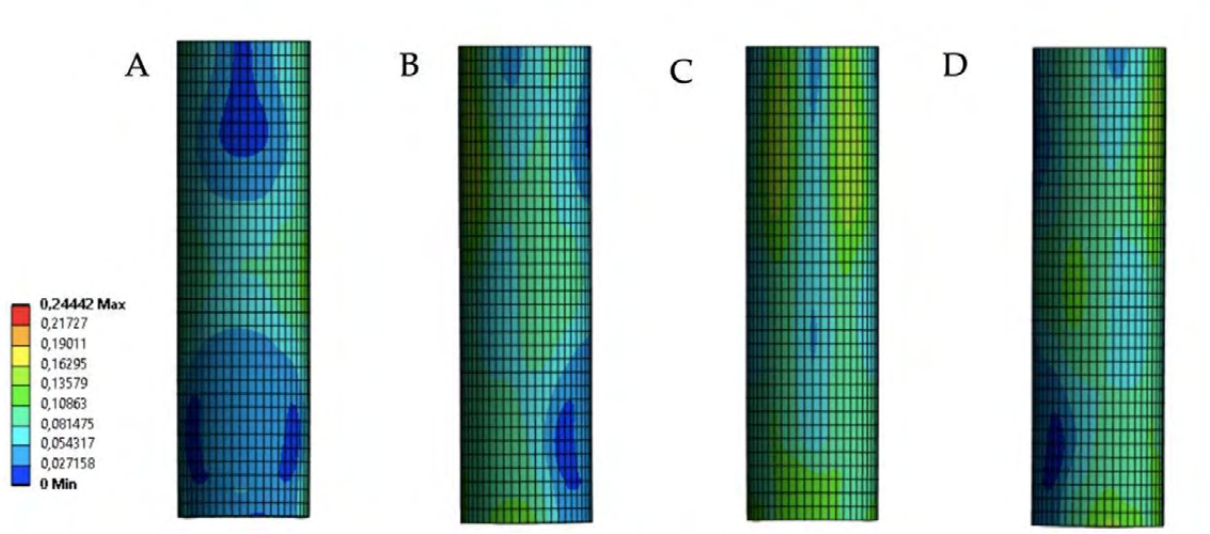

Figure 12. Maximum deformation of an aortic wall in healthy conditions at the speed of 30 km/h. A — aortic front wall; B — left wall; C — posterior wall; D — right wall

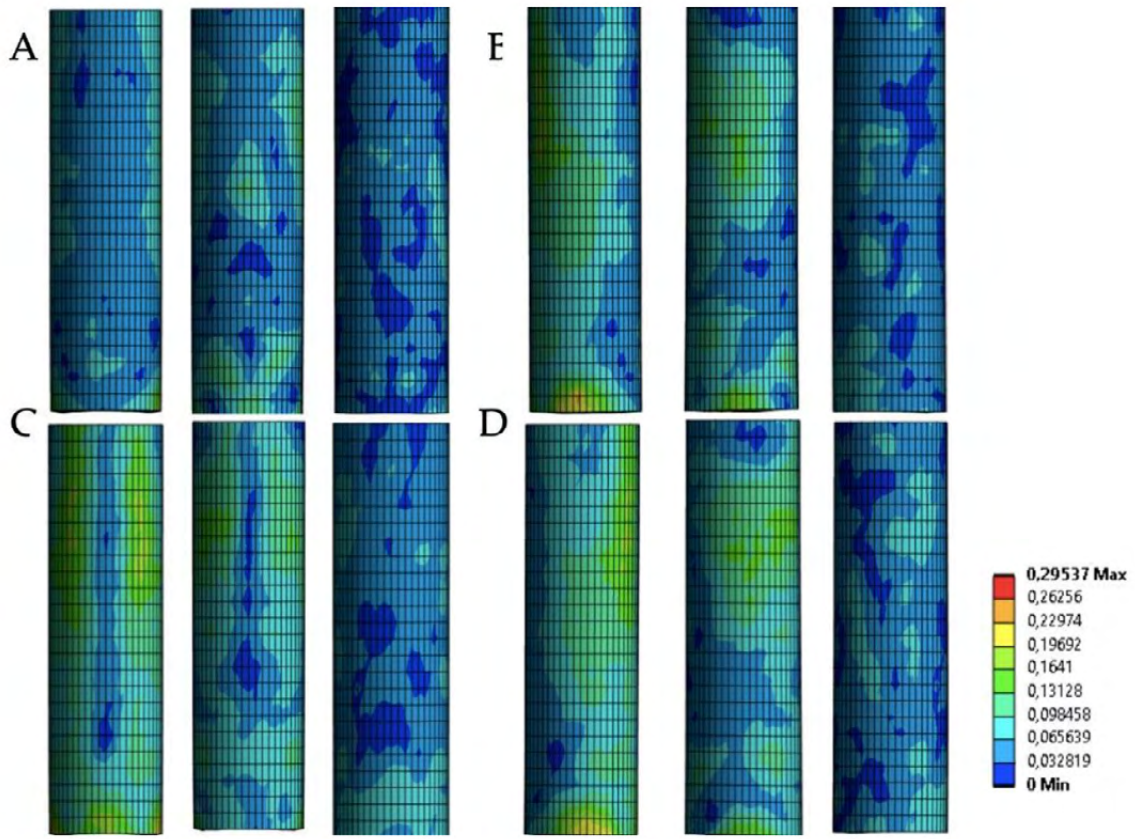

Figure 13. Maximum stresses in an aortic wall in stage 1 within the first second after impact at 30 km/h. A — aortic front wall; B — left wall; C — posterior wall; D — right wall

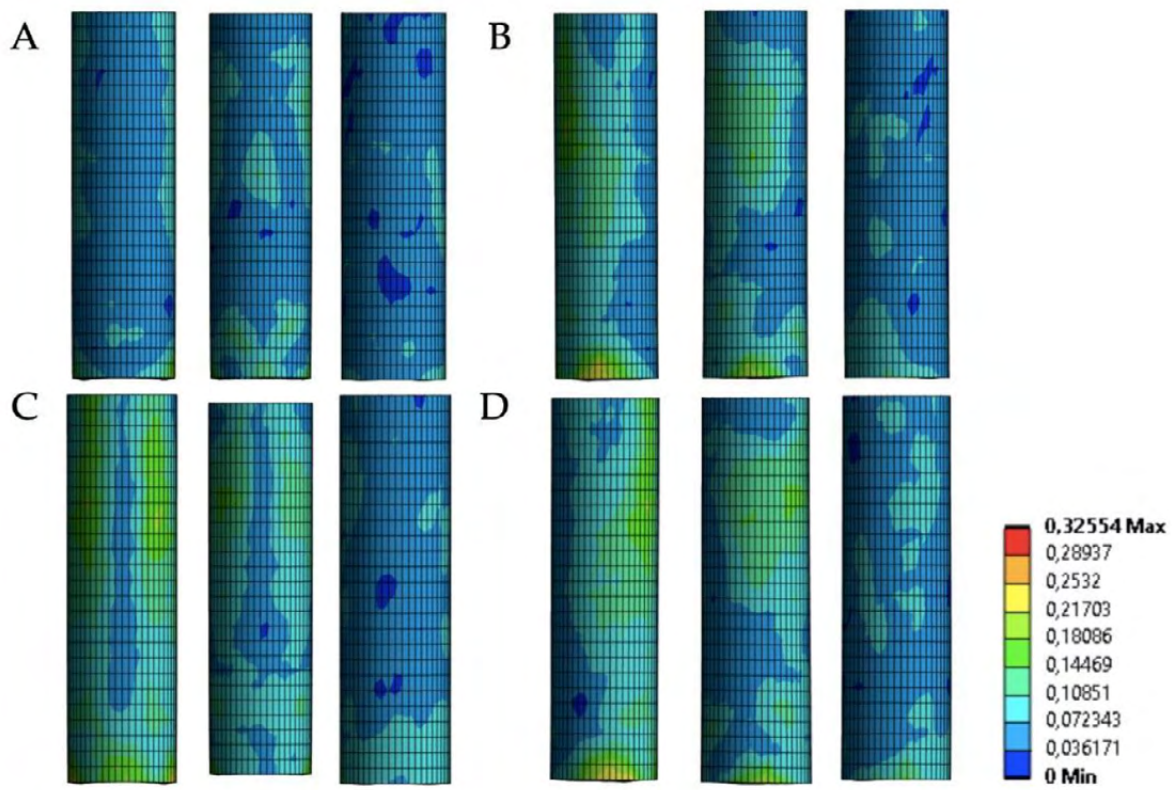

Figure 14. Maximum deformation of an aortic wall in stage 1 within the first second after impact at 30 km/h. A — aortic front wall; B — left wall; C — posterior wall; D — right wall

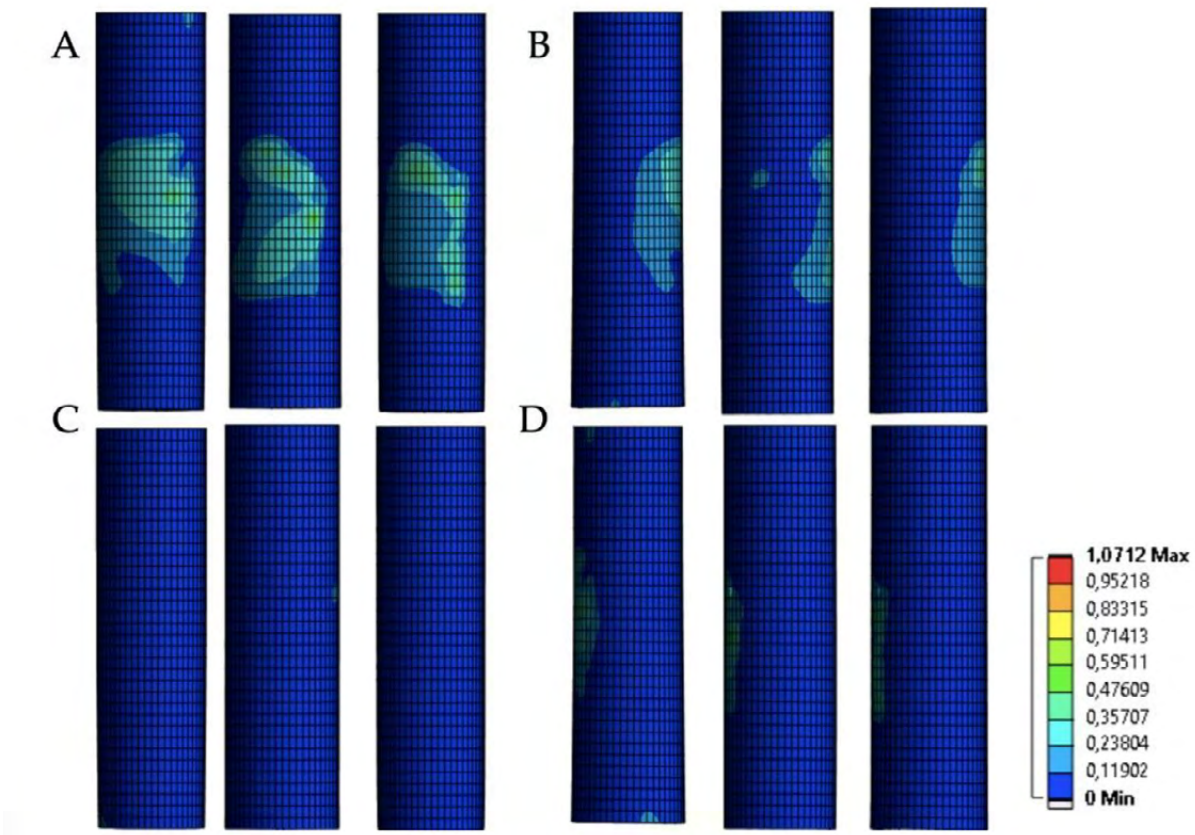

Figure 15. Maximum stresses in an aortic wall in stage 4 within the first second after impact at 30 km/h. A — aortic front wall; B — left wall; C — posterior wall; D — right wall

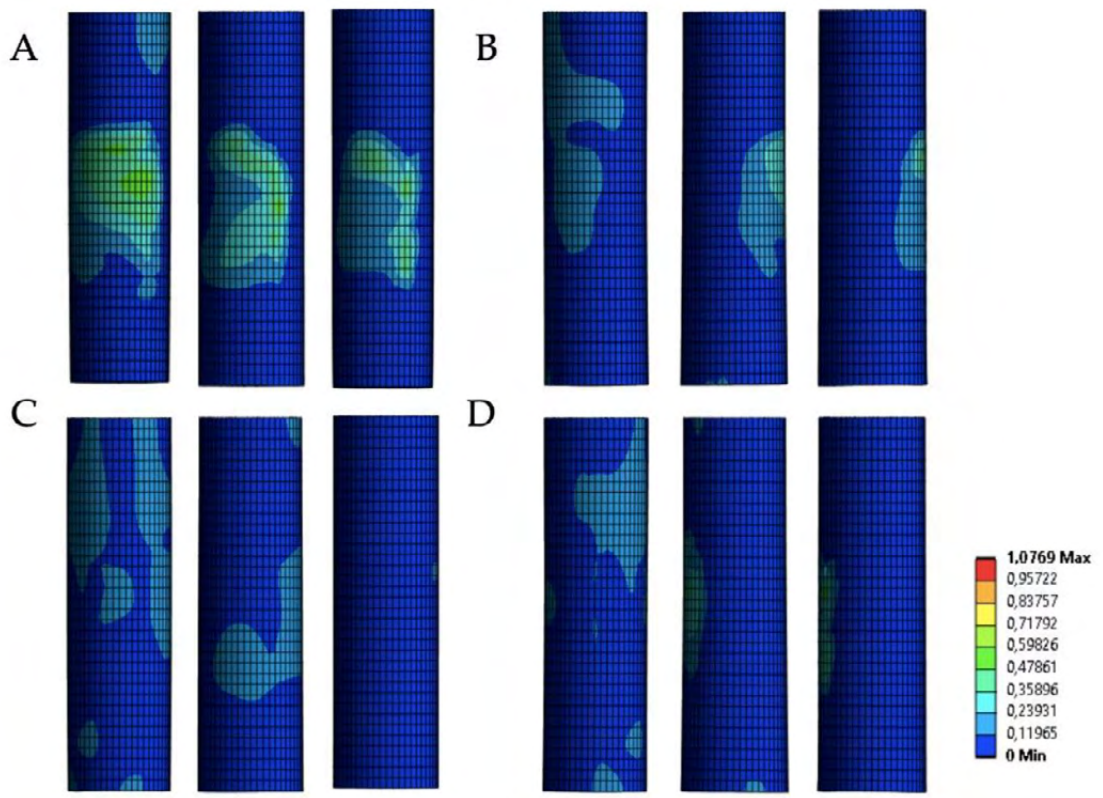

Figure 16. Maximum deformation of an aortic wall in in stage 4 within the first second after impact at 30 km/h. A — aortic front wall; B — left wall; C — posterior wall; D — right wall

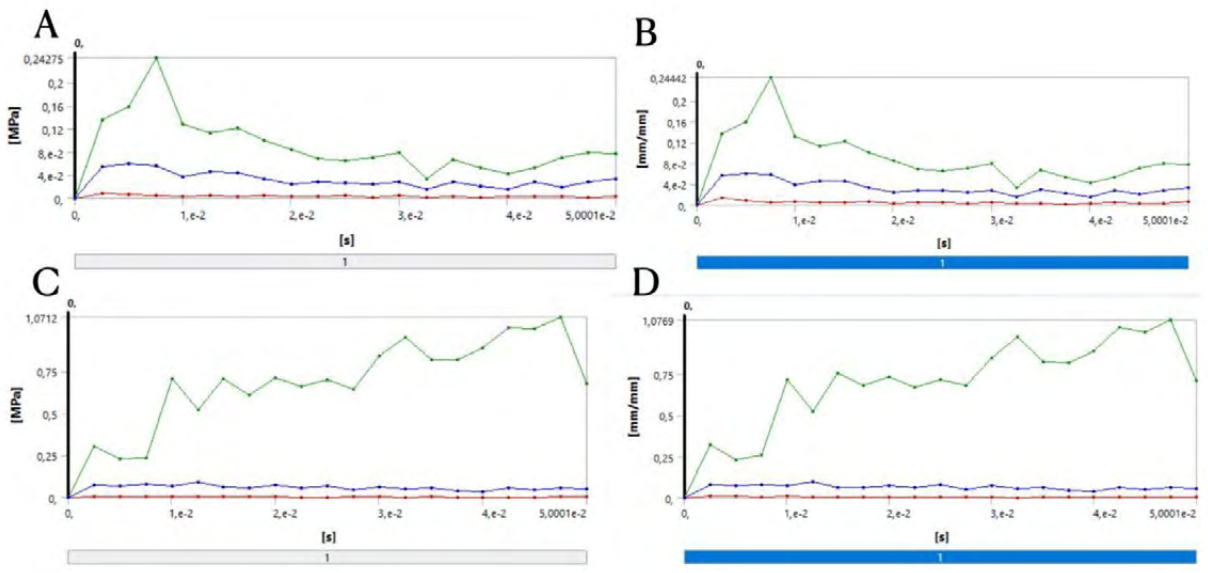

Figure 17. Speed of 30 km/h in healthy condition: A) stresses; B) deformations. Speed of 30 km/h in Stage 4: C) stresses; D) deformations

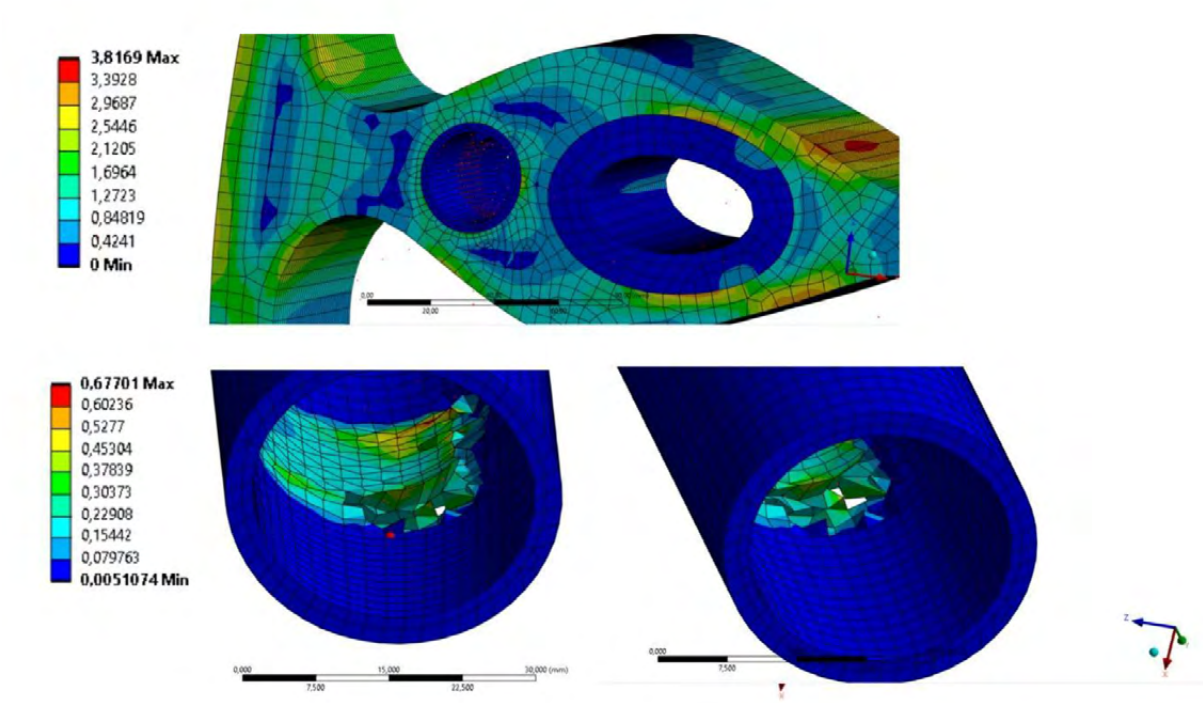

Figure 18. Aortic rupture in stage 4 at a speed of 30 km/h

Article information and declarations

Data availability statement: The data that support the findings of this study are available on request from the corresponding author.

Ethics statement: The study protocol conforms to the ethical guidelines of the 1975 Declaration of Helsinki. Approval of the institutional ethics commission has been obtained for this study (Decision number 33/2019 of 13.02.2019).

Author contributions: Concept, visualization, methodology, results, manuscript preparation, review — O.K., J.L.; methodology, results — L.L.

Funding: This study received no funding.

Conflict of interest: The authors declare no conflict of interest.

References

1. Zhao AR, Field ML, Digges K, et al. Blunt trauma and acute aortic syndrome: a three-layer finite-element model of the aortic wall. Eur J Cardiothorac Surg. 2008; 34(3): 623–629, doi: 10.1016/j.ejcts.2008.02.032, indexed in Pubmed: 18539473.
2. Siegel JH, Belwadi A, Smith JA, et al. Analysis of the mechanism of lateral impact aortic isthmus disruption in real-life motor vehicle crashes using a computer-based finite element numeric model: with simulation of prevention strategies. J Trauma. 2010; 68(6): 1375–1395, doi: 10.1097/TA.0b013e3181dcd42d, indexed in Pubmed: 20539183.
3. Mohamied Y, Rowland EM, Bailey EL, et al. Change of direction in the biomechanics of atherosclerosis. Ann Biomed Eng. 2015; 43(1): 16–25, doi: 10.1007/s10439-014-1095-4, indexed in Pubmed: 25138165.
4. Lacolley P, Regnault V, Avolio AP. Smooth muscle cell and arterial aging: basic and clinical aspects. Cardiovasc Res. 2018; 114(4): 513–528, doi: 10.1093/cvr/cvy009, indexed in Pubmed: 29514201.
5. Kozuń M, Kobielarz M, Chwiłkowska A, et al. The impact of development of atherosclerosis on delamination resistance of the thoracic aortic wall. J Mech Behav Biomed Mater. 2018; 79: 292–300, doi: 10.1016/j.jmbbm.2018.01.009, indexed in Pubmed: 29353772.
6. Holzapfel GA, Gasser TC, Ogden RW. Comparison of a multi-layer structural model for arterial walls with a fung-type model, and issues of material stability. J Biomech Eng. 2004; 126(2): 264–275, doi: 10.1115/1.1695572, indexed in Pubmed: 15179858.
7. Kobielarz M, Kozuń M, Gąsior-Głogowska M, et al. Mechanical and structural properties of different types of human aortic atherosclerotic plaques. J Mech Behav Biomed Mater. 2020; 109: 103837, doi: 10.1016/j.jmbbm.2020.103837, indexed in Pubmed: 32543403.
8. Erbel R, Aboyans V, Boileau C, et al. ESC Committee for Practice Guidelines. 2014 ESC Guidelines on the diagnosis and treatment of aortic diseases: Document covering acute and chronic aortic diseases of the thoracic and abdominal aorta of the adult. The Task Force for the Diagnosis and Treatment of Aortic Diseases of the European Society of Cardiology (ESC). Eur Heart J. 2014; 35(41): 2873–2926, doi: 10.1093/eurheartj/ehu281, indexed in Pubmed: 25173340.

9. Jiang CP, Wibisono AT, Pasang T. Selective laser melting of stainless steel 316L with face-centered-cubic-based lattice structures to produce rib implants. Materials (Basel). 2021; 14(20), doi: 10.3390/ma14205962, indexed in Pubmed: 34683551.
10. Jansova, Magdalena & Hyncik, Ludek & Cechova, Hana & Toczyski, Jacek & Gierczycka-Zbrozek, Donata & Baudrit, Pascal. Evaluation of human thorax FE model in various impact scenarios. Applied and Computational Mechanics. 2015; 9: 5–20.
11. Giambini H, Wang HJ, Zhao C, et al. Anterior and posterior variations in mechanical properties of human vertebrae measured by nanoindentation. J Biomech. 2013; 46(3): 456–461, doi: 10.1016/j.jbiomech.2012.11.008, indexed in Pubmed: 23182219.
12. Gao F, Watanabe M, Matsuzawa T. Stress analysis in a layered aortic arch model under pulsatile blood flow. Biomed Eng Online. 2006; 5: 25, doi: 10.1186/1475-925X-5-25, indexed in Pubmed: 16630365.
13. Huyer LD, Montgomery M, Zhao Y, et al. Biomaterial based cardiac tissue engineering and its applications. Biomed Mater. 2015; 10(3): 034004, doi: 10.1088/1748-6041/10/3/034004, indexed in Pubmed: 25989939.
14. Emig R, Zgierski-Johnston CM, Timmermann V, et al. Passive myocardial mechanical properties: meaning, measurement, models. Biophys Rev. 2021; 13(5): 587–610, doi: 10.1007/s12551-021-00838-1, indexed in Pubmed: 34765043.
15. Dulińska I, Targosz M, Strojny W, et al. Stiffness of normal and pathological erythrocytes studied by means of atomic force microscopy. J Biochem Biophys Methods. 2006; 66(1-3): 1–11, doi: 10.1016/j.jbbm.2005.11.003, indexed in Pubmed: 16443279.
16. Kim Y, Kim K, Park Y. Measurement techniques for red blood cell deformability: recent advances. Blood Cell - An Overview of Studies in Hematology. 2012, doi: 10.5772/50698.
17. Habibi R, Devendran C, Neild A. Trapping and patterning of large particles and cells in a 1D ultrasonic standing wave. Lab Chip. 2017; 17(19): 3279–3290, doi: 10.1039/c7lc00640c, indexed in Pubmed: 28840206.
18. Al-Mayah A, Moseley J, Velec M, et al. Sliding characteristic and material compressibility of human lung: parametric study and verification. Med Phys. 2009; 36(10): 4625–4633, doi: 10.1118/1.3218761, indexed in Pubmed: 19928094.
19. Zeng YJ, Yager D, Fung YC. Measurement of the mechanical properties of the human lung tissue. J Biomech Eng. 1987; 109(2): 169–174, doi: 10.1115/1.3138661, indexed in Pubmed: 3599944.
20. Noferest BS. Inverse-Consistent Determination of Young's Modulus of Human Lung. Electronic Theses and Dissertations. 2015; 5149.
21. Hajhosseini P, Takalloozadeh M. An isotropic hyperelastic model of esophagus tissue layers along with three-dimensional simulation of esophageal peristaltic behavior. Journal of Bioengineering Research. 2019; 1(2): 12–27, doi: 10.22034/jbr.2019.189018.1009.
22. Comley K, Fleck N. A micromechanical model for the Young's modulus of adipose tissue. Int J Solids Struct. 2010; 47(21): 2982–2990, doi: 10.1016/j.ijsolstr.2010.07.001.
23. Carrera E, Guarnera D, Pagani A. Static and free-vibration analyses of dental prosthesis and atherosclerotic human artery by refined finite element models. Biomech Model Mechanobiol. 2018; 17(2): 301–317, doi: 10.1007/s10237-017-0961-z, indexed in Pubmed: 28905122.
24. Yang KH, Hu J, White NA, et al. Development of numerical models for injury biomechanics research: a review of 50 years of publications in the Stapp Car Crash Conference. Stapp Car Crash J. 2006; 50: 429–490, doi: 10.4271/2006-22-0017, indexed in Pubmed: 17311173.
25. Wang, Hui-Chang Kevin. Development of a side impact finite element human thoracic model [PhD thesis]. MI: Wayne State University, Detroit 1995.
26. Shah CS, Yang KH, Hardy W, et al. Development of a computer model to predict aortic rupture due to impact loading. Stapp Car Crash J. 2001; 45: 161–182, doi: 10.4271/2001-22-0007, indexed in Pubmed: 17458744.
27. Khosravi A, Bani MS, Bahreinizade H, et al. A computational fluid-structure interaction model to predict the biomechanical properties of the artificial functionally graded aorta. Biosci Rep. 2016; 36(6), doi: 10.1042/BSR20160468, indexed in Pubmed: 27836981.
28. Dabagh M, Jalali P, Konttinen YT, et al. Distribution of shear stress over smooth muscle cells in deformable arterial wall. Med Biol Eng Comput. 2008; 46(7): 649–657, doi: 10.1007/s11517-008-0338-7, indexed in Pubmed: 18386089.
29. Towfiq BA, Weir J, Rawles JM. Effect of age and blood pressure on aortic size and stroke distance. Br Heart J. 1986; 55(6): 560–568, doi: 10.1136/hrt.55.6.560, indexed in Pubmed: 3718794.
30. Wolak A, Gransar H, Thomson LEJ, et al. Aortic size assessment by noncontrast cardiac computed tomography: normal limits by age, gender, and body surface area. JACC Cardiovasc Imaging. 2008; 1(2): 200–209, doi: 10.1016/j.jcmg.2007.11.005, indexed in Pubmed: 19356429.
31. Vasava P, Jalali P, Dabagh M, et al. Finite element modelling of pulsatile blood flow in idealized model of human aortic arch: study of hypotension and hypertension. Comput Math Methods Med. 2012; 2012: 861837, doi: 10.1155/2012/861837, indexed in Pubmed: 22400055.
32. Grave-Capistrán MA, Prieto-Vázquez AY, Torres-San-Miguel CR. Aortic Blunt Trauma Analysis during a Frontal Impact. Appl Bionics Biomech. 2021; 2021: 5555218, doi: 10.1155/2021/5555218, indexed in Pubmed: 34335871.
33. Siegel JH, Yang KH, Smith JA, et al. Computer simulation and validation of the Archimedes Lever hypothesis as a mechanism for aortic isthmus disruption in a case of lateral impact motor vehicle crash: a Crash Injury Research Engineering Network (CIREN) study. J Trauma. 2006; 60(5): 1072–1082, doi: 10.1097/01.ta.0000203542.38532.02, indexed in Pubmed: 16688073.
34. Richens D, Field M, Hashim S, et al. A finite element model of blunt traumatic aortic rupture. Eur J Cardiothorac Surg. 2004; 25(6): 1039–1047, doi: 10.1016/j.ejcts.2004.01.059, indexed in Pubmed: 15145007.
35. Belwadi A, Siegel JH, Singh A, et al. Finite element aortic injury reconstruction of near side lateral impacts using real world crash data. J Biomech Eng. 2012; 134(1): 011006, doi: 10.1115/1.4005684, indexed in Pubmed: 22482661.
36. Hardy WN, Shah CS, Mason MJ, et al. Mechanisms of traumatic rupture of the aorta and associated peri-isthmic motion and deformation. Stapp Car Crash J. 2008; 52: 233–265, doi: 10.4271/2008-22-0010, indexed in Pubmed: 19085165.

37. Richens D, Field M, Neale M, et al. The mechanism of injury in blunt traumatic rupture of the aorta. Eur J Cardiothorac Surg. 2002; 21(2): 288–293, doi: 10.1016/s1010-7940(01)01095-8, indexed in Pubmed: 11825737.
38. Stary HC, Chandler AB, Dinsmore RE, et al. A definition of advanced types of atherosclerotic lesions and a histological classification of atherosclerosis. A report from the Committee on Vascular Lesions of the Council on Arteriosclerosis, American Heart Association. Circulation. 1995; 92(5): 1355–1374, doi: 10.1161/01.cir.92.5.1355, indexed in Pubmed: 7648691.
39. Stary HC, Chandler AB, Glagov S, et al. A definition of initial, fatty streak, and intermediate lesions of atherosclerosis. A report from the Committee on Vascular Lesions of the Council on Arteriosclerosis, American Heart Association. Arterioscler Thromb. 1994; 14(5): 840–856, doi: 10.1161/01.atv.14.5.840, indexed in Pubmed: 8172861.
40. Sznol JA, Koru-Sengul T, Graygo J, et al. Etiology of fatal thoracic aortic injuries: Secondary data analysis. Traffic Inj Prev. 2016; 17(2): 209–216, doi: 10.1080/15389588.2015.1067805 , indexed in Pubmed: 26605433.
41. Lorkowski J, Kolaszyńska O, Pokorski M. Artificial intelligence and precision medicine: a perspective. Adv Exp Med Biol. 2022; 1375: 1–11, doi: 10.1007/5584_2021_652, indexed in Pubmed: 34138457.
42. Liang L, Liu M, Elefteriades J, et al. Synergistic integration of deep neural networks and finite element method with applications for biomechanical analysis of human aorta. bioRxiv. 2023, doi: 10.1101/2023.04.03.535423, indexed in Pubmed: 37066215.
43. McKee CT, Last JA, Russell P, et al. Indentation versus tensile measurements of Young's modulus for soft biological tissues. Tissue Eng Part B Rev. 2011; 17(3): 155–164, doi: 10.1089/ten.TEB.2010.0520, indexed in Pubmed: 21303220.
44. Horton TG, Cohn SM, Heid MP, et al. Identification of trauma patients at risk of thoracic aortic tear by mechanism of injury. J Trauma. 2000; 48(6): 1008–13; discussion 1013, doi: 10.1097/00005373-200006000-00003, indexed in Pubmed: 10866244.
45. Lorenzo AH, Wilhelmi M, Anduaga AM. Traumatismo torácico y rotura aórtica. Puesta al día en urgencias, emergencias y catástrofes. 2009; 9: 134–145.